Searching for the source regions of martian meteorites using MGS TES: Integrating martian meteorites into the global distribution of igneous materials on Mars

Victoria E. HAMILTON,[1*] Philip R. CHRISTENSEN,[2] Harry Y. McSWEEN, Jr.,[3] and Joshua L. BANDFIELD[2]

[1]Hawai'i Institute of Geophysics and Planetology, University of Hawai'i, Honolulu, Hawai'i 96822, USA
[2]Department of Geological Sciences, Arizona State University, Tempe, Arizona 85287–6305, USA
[3]Department of Earth and Planetary Sciences, University of Tennessee, Knoxville, Tennessee 37996–1410, USA
[*]Corresponding author. E-mail: hamilton@higp.hawaii.edu

Abstract–The objective of this study was to identify and map possible source regions for all 5 known martian meteorite lithologies (basalt, lherzolite, clinopyroxenite, orthopyroxenite, and dunite) using data from the Mars Global Surveyor Thermal Emission Spectrometer (MGS TES). We deconvolved the TES data set using laboratory spectra of 6 martian meteorites (Los Angeles, Zagami, ALH A77005, Nakhla, ALH 84001, and Chassigny) as end members, along with atmospheric and surface spectra previously derived from TES data. Global maps (16 pixels/degree) of the distribution of each meteorite end member show that meteorite-like compositions are not present at or above TES detectability limits over most of the planet's dust-free regions. However, we have confidently identified local-scale (100s–1000s km^2) concentrations of olivine- and orthopyroxene-bearing materials similar to ALH A77005, Chassigny, and ALH 84001 in Nili Fossae, in and near Ganges Chasma, in the Argyre and Hellas basin rims, and in Eos Chasma. Nakhla-like materials are identified near the detection limit throughout the eastern Valles Marineris region and portions of Syrtis Major. Basaltic shergottites were not detected in any spatially coherent areas at the scale of this study. Martian meteorite-like lithologies represent only a minor portion of the dust-free surface and, thus, are not representative of the bulk composition of the ancient crust. Meteorite-like spectral signatures identified above TES detectability limits in more spatially restricted areas (<tens of km) are targets of ongoing analysis.

INTRODUCTION AND BACKGROUND

Although much is known about martian meteorites (and thus, Mars) from detailed studies of their mineralogy and chemistry, they cannot be placed into the appropriate geologic context because we do not know where they originated on the planet's surface. Locating one or more source regions would provide valuable contextual information, might permit a better understanding of the meteorites' ejection ages and the number of ejection events, and allow (in the best possible case) an absolute age calibration to the crater count chronology of Mars. The Thermal Emission Spectrometer (TES) provides a high spectral and spatial resolution global data set that can be used to search for possible source regions of these meteorites. This work is a first effort to identify possible martian meteorite source regions based on TES data. We first review prior attempts to describe likely parent craters based on the meteorites' characteristics and on ejection dynamics, prior spectroscopic evidence for meteorite-like lithologies on Mars, and lithologies previously identified by the TES instrument.

The Approach section describes our approach to TES data analysis, and the Results and Discussion section presents our major results and discussion. The section, Integrating Martian Meteorites and Martian Geology, attempts to put our observations into the context of what is known about Mars from in situ and meteorite data, and the Conclusions section summarizes our major conclusions.

Constraints on and Past Searches for SNC Source Regions on Mars

Martian meteorites, also commonly referred to as SNCs (shergottites, nakhlites, and Chassigny), are achondrites of varying mafic to ultramafic igneous lithologies, exhibiting both intrusive and extrusive textures including: basalt and lherzolite (shergottites), orthopyroxenite (ALH 84001), clinopyroxenite (nakhlites), and dunite (Chassigny). Several lines of evidence (recently summarized by Treiman et al. [2000] and Nyquist et al. [2001]) strongly suggest Mars is the parent body of these meteorites.

Numerous investigators have attempted to identify possible source regions for the martian meteorites by using their ages and current knowledge of cratering dynamics to constrain geologically and chronologically appropriate terrains (and craters) on Mars (Wood and Ashwal 1981; Schultz and Lutz-Garihan 1982; Nyquist 1983; Jones 1985; McSween 1985; Mouginis-Mark et al. 1992; Treiman 1995; Barlow 1997; Rice 1997; Nyquist et al. 1998). Martian meteorites, with the exception of ALH 84001, are relatively young, with crystallization ages ranging from 175 Ma to 1.3 Ga (Nyquist et al. 2001 and references therein). These ages correspond to the Amazonian period on Mars and typically have been used to infer that the source region should be a geologically young surface, such as is found in much of the Tharsis and Elysium regions.

The ejection ages of the meteorites, based on cosmic ray exposure data (e.g., Eugster et al. 1997), constrain the likely parent crater ages and morphologies (e.g., Mouginis-Mark et al. 1992). Many investigators have attempted to discern how many events were required to eject the SNC meteorites (Wood and Ashwal 1981; Nyquist 1983; Bogard et al. 1984; Vidal 1984; McSween 1985; Jones 1986; Vickery and Melosh 1987; Mouginis-Mark et al. 1992). Revisions of the meteorites' crystallization ages and ejection ages, as well as further insight into their chemistries, now appear to indicate that multiple ejection events are required between ~20 and 0.7 Ma (e.g., Treiman 1995; Eugster et al. 1997; Nyquist et al. 1998; 2001).

Many studies of cratering dynamics have attempted to describe the dimensions of a crater resulting from an impact capable of ejecting martian materials into an Earth-crossing orbit (Nyquist 1983, 1984; Melosh 1985; O'Keefe and Ahrens 1986; Vickery and Melosh 1987; Warren 1994; Gladman 1997; Head 1999; Head and Melosh 2000; Mileikowsky et al. 2000; Head et al. 2002). Early work indicated that favored candidate craters would be ~100–200 km in diameter and/or that oblique impacts might be required to eject materials from Mars' gravity field, but the most recent estimates have revised the minimum size of circular craters to ~3 km.

Previous Spectroscopic Evidence for SNC-Like Materials on Mars

Early visible and near-infrared reflectance spectra from telescopic observations of martian dark (albedo <~0.24) regions showed ~1.0 and 2.0 μm absorption features interpreted to indicate the presence of mafic mineralogies (e.g., Adams and McCord 1969; Singer 1980; Singer and McSween 1993). More recent data collected by the Imaging Spectrometer for Mars (ISM) experiment aboard the Soviet Phobos 2 spacecraft are consistent with these earlier interpretations, identifying a pyroxene component (Bibring et al. 1990; Mustard et al. 1993), specifically, a combination of high- and low-calcium pyroxene (likely augite and pigeonite

[Mustard and Sunshine 1995]). These pyroxenes are present in relative abundances consistent with the relative abundances of high- and low-calcium pyroxene in some basaltic shergottites (Mustard and Sunshine 1995; Mustard et al. 1997).

Mars Global Surveyor Thermal Emission Spectrometer (MGS TES)

The MGS TES has a spectral range of ~1650–200 cm^{-1} (~6–50 μm) and a spatial resolution of approximately 3×6 km. A detailed description of the instrument can be found in Christensen et al. (1992, 2001a). Thermal IR spectroscopy is useful for remotely determining mineralogy because virtually all minerals have unique spectral signatures resulting from fundamental vibrations in the thermal IR portion of the electromagnetic spectrum. The compositions of dark regions on Mars have been identified from MGS TES data and are characterized as dominated by a basaltic component (surface type 1), crystalline hematite, and/or a component (surface type 2) that was identified as basaltic andesite, andesite, or partially weathered basalt (Bandfield et al. 2000; Christensen et al. 2000a; Christensen et al. 2000b; Hamilton et al. 2001c; Wyatt and McSween 2002). (Although there is debate as to the interpretation of the latter surface type, the terms "intermediate" or "andesitic" are used here.) Recent results (Clark and Hoefen 2000; Hoefen et al. 2000; Hamilton et al. 2001a; Ruff and Hamilton 2001; Hamilton et al. 2002) indicate that smaller spatial scale variations in composition are observable, including the identification of olivine in Nili Fossae (NE of Syrtis Major), in craters near Ganges Chasma, and at the rims of the Argyre and Hellas basins (Clark and Hoefen 2000; Hoefen et al. 2000; Hamilton et al. 2001a, 2001b, 2002).

APPROACH

Linear Deconvolution

Spectra of Mars acquired by TES are resolved into constituent rock or mineral contributions via the linear deconvolution technique and error analysis of Ramsey and Christensen (1998). Linear deconvolution is based on the principle that the spectrum of a rock (mixture) is a linear combination of the spectra of the minerals composing the rock (mixture), in proportion to their abundance (Lyon 1965; Christensen et al. 1986; Crown and Pieters 1987; Thomson and Salisbury 1993). A linear deconvolution algorithm uses a library of mineral or rock spectra ("end members") to perform an iterative, linear least squares fit to the spectrum of an unknown mixture. The term "end member" in this usage does not necessarily imply chemical purity (i.e., a solid solution end member) or a single mineral, although these are possibilities. Rather, an end member is similar to a "pure

pixel" in remote sensing image analysis, where the pure pixel represents a spectral component that is not intermixed with other components within the image. Upon obtaining a fit to the unknown spectrum, the algorithm supplies the user with a model-derived spectrum and the percentage of each end member used in the fit (end members with negative percentages are removed during the iterative process because they are geologically meaningless). The percentages represent areal abundances and are comparable to viewing a rock in thin section. The quality and accuracy of the fit and modeled mineralogy can be evaluated mathematically by taking the difference between the model-derived spectrum and the unknown spectrum as well as by the root-mean-square (RMS) error value provided in the output of the algorithm (Hamilton et al. 1997; Ramsey and Christensen 1998; Feely and Christensen 1999; Hamilton and Christensen 2000). The algorithm can use only the end members provided by the user; if a significant component of the unknown material is not provided as an end member, the deconvolution cannot identify it and will make the best fit possible with the available end members. In such cases, high RMS errors are likely. Laboratory studies show that, for well-characterized rock samples or particulate mixtures, individual phases are confidently detected at abundances greater than ~5 vol%, with some variation in the accuracies of various mineral phases (Hamilton et al. 1997; Ramsey and Christensen 1998; Feely and Christensen 1999; Hamilton and Christensen 2000; Wyatt et al. 2001).

The end members used in this study consist of meteorite, atmospheric, and typical Mars surface spectra. The meteorite samples analyzed for this study were obtained from a variety of sources and all are solid pieces. The Zagami sample is from the private collection of one of the authors (PRC) and is from the "normal" Zagami lithology (i.e., no olivine). Los Angeles 2–1418 is a piece of stone 1 (Rubin et al. 2000) provided by the Arizona State University (ASU) Center for Meteorite Studies. The Smithsonian Institution provided our Nakhla sample (USNM 426). Although the modal mineralogy for this particular Nakhla stone has not been determined, deconvolution analyses of its spectrum identify approximately 10 vol% olivine (Hamilton et al. 1997; Hamilton, unpublished data), suggesting that it is not one of the stones rich in olivine (Friedman Lentz et al. 1999). The Center for Antarctic Meteorite Studies at the Johnson Space Center provided ALH A77005, splits 77 and 65, as well as split 274 of ALH 84001. The sample of Chassigny was provided by the Center for Meteorite Studies at ASU. All meteorite spectra were acquired at ASU with a Nicolet Nexus 670 FTIR spectrometer that measures sample emissivity from ~2000–220 cm^{-1} (~5–45 μm) at 2 cm^{-1} spectral sampling; data acquisition followed the physical set up and calibration described by Ruff et al. (1997) and Christensen and Harrison (1993). Spot sizes of ~1 cm were observed on each sample, ensuring a representative spectrum. The spectra of each meteorite are shown in Fig. 1.

The nature of the orbital measurement dictates atmospheric components (dust, water ice clouds, CO_2 gas) will contribute to the TES spectra. To interpret the spectral features on the surface, these atmospheric components must be identified and isolated. Smith et al. (2000) have shown that, to first order, a spectrum containing atmospheric and surface components can be modeled as a linear mixture. Therefore, spectra of the atmospheric components (derived from TES data) are also included as end members.

Other end members used in the deconvolution of TES data include the basaltic, intermediate, and hematite-bearing surfaces identified by Bandfield et al. (2000) and Christensen et al. (2000a). Because laboratory data are acquired at higher spectral resolution than are TES data, the laboratory data are resampled to TES resolution. The TES data are deconvolved over the wavelength ranges of ~1300–825 cm^{-1} and ~508–232 cm^{-1} simultaneously, thus excluding the region of the fundamental CO_2 atmospheric absorption (Bandfield et al. 2000).

In describing deconvolution results from martian data that include atmospheric components, we refer to end
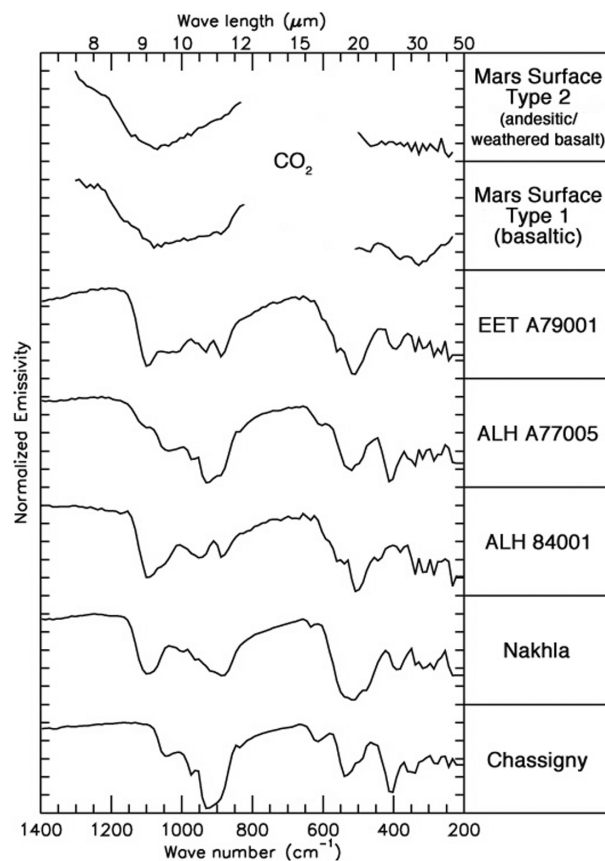

Fig. 1. Thermal infrared emission spectra of martian meteorites compared to spectra of igneous surface components observed by the TES at Mars. The region of atmospheric CO_2 absorption is excluded in the TES spectra and lab spectra are shown at the same spectral resolution as the TES data.

member concentrations, which we define as the fractional contribution to the total spectral signal. To refer to the quantities of components on the surface, we subtract the concentrations of the atmospheric components, normalize the surface component fractions to 100%, and use the term abundance. Detection limits associated with martian data are somewhat higher than for laboratory data due to the lower spectral resolution and decreased signal of the orbital instrument as compared to the laboratory spectrometer. Concentrations of 0.10 are the minimum detection limit previously identified for martian data (Bandfield et al. 2000; Christensen et al. 2000b; Bandfield 2002).

TES Data Selection

For this study, we selected TES day side data from the nominal mission and early extended mission (TES OCKs 1583–9500; Ls = 103.5° to 85.8°) with surface temperatures greater than 255 K and low emission angles (<10°) for the highest signal to noise. We included only single-scan (10 cm^{-1} sampling), full spectral, full spatial resolution data in our analysis. The number of spectra analyzed is on the order of 10– 20×10^6. Data in regions with high Lambert albedo (>0.24 integrated over the region 0.3–3.3 μm by the TES visible bolometer) were not included in our analysis because high albedo surfaces are generally dust-covered and will not be modeled correctly by end member spectra of coarse particulate or solid samples, which are used here (Ramsey and Christensen 1998). We used information available in the TES database to further exclude data at risk for increased noise resulting from solar panel and high-gain antenna (HGA) motion and errors due to major phase inversions.

Global Mapping

As the first step in searching the TES data set for spectral signatures like those of martian meteorites, we used a deconvolution and mapping strategy like that of Bandfield et al. (2000), who used primary martian (atmospheric and surface) spectral end members to deconvolve the TES data set and then used the deconvolution results to create global maps of the distributions of the surface materials. To the TES atmospheric and surface end members, we added 6 meteorite spectra representative of the 5 major classes of martian meteorites (described above under Linear Deconvolution). The decision to use these meteorite spectra as end members was motivated in part by the simplicity of the approach and also by the lack of pure mineral end member spectra exactly replicating the mineral compositions in the meteorites themselves, particularly low-calcium augites and Mg-rich pigeonite. By using the meteorite spectra, we used a similar approach to that taken by Bandfield et al. (2000) ("unit" or "lithology" mapping) and we ensured that we were using spectra that exactly represent the mineralogies of the meteorites. We deconvolved individual pixels in the TES data set and made global maps (binned at 16 pixels per degree) of the retrieved concentration of each meteorite end member.

Another possible means of identifying meteorite-like lithologies at global scales is to use spectra of each meteorite to identify distinctive features that can be used to create band depth indices (e.g., [emissivity of band x + emissivity of band z]/(emissivity of band y]) that can be calculated for all TES spectra and mapped. A significant disadvantage of the band index approach is that instead of locating a match to all of the features in the spectrum of interest (as in deconvolution), only a few bands of the entire spectrum are being matched and may not yield a unique identification if another material, combination of materials, or atmospheric component has similar features over the selected spectral subregion. Test maps based on indices for Chassigny and ALH 84001 were created and, as expected, did not reveal significant occurrences that were not already identified by mapping the deconvolution-derived abundances, and some spurious data were identified. Because of the potential pitfalls of index mapping, we have chosen to avoid this approach in our study.

RESULTS AND DISCUSSION

Global maps (16 pixels/degree) of the distributions of surface end members are available at http://www.higp.hawaii.edu/~hamilton/snc_maps.html. We first compared our global maps of the basaltic, intermediate, and hematite-bearing surface types to the maps of Bandfield et al. (2000) and Christensen et al. (2001b) to verify our basic results. We find good agreement between all datasets, indicating that we have not unintentionally introduced any significant errors into the data analysis stream. The map of RMS error (also at the website above) for these deconvolutions shows that the highest values (=1%, or 0.01 emissivity) are typically correlated with areas of relatively high albedo (>0.20), as expected, and the lowest RMS values (<0.5%) are found in the lowest albedo regions.

Our global maps of the derived abundance of each of the six meteorite spectral end members confirm that spectral shapes resembling those of the martian meteorites do not dominate spatially extensive (1,000,000s km^2) dark regions on Mars. However, several local (100s–1000s km^2) areas have been identified where concentrations of some of these end members were identified at or above TES detectability limits in multiple pixels. The locations of sites described in detail in this paper are shown schematically in Fig. 2. We made higher resolution maps (32 pixels/degree) and manually inspected representative spectral data in these areas using a variety of approaches (described below) to ensure that no problems with the spectra, such as excessive noise, were causing erroneous identifications. In the present work, we did not consider single-pixel detections (either at the binned 16 pixel/degree or full spatial resolution scales). Note that use of a meteorite end member in a model fit does not necessarily imply that the surface component is martian meteorite
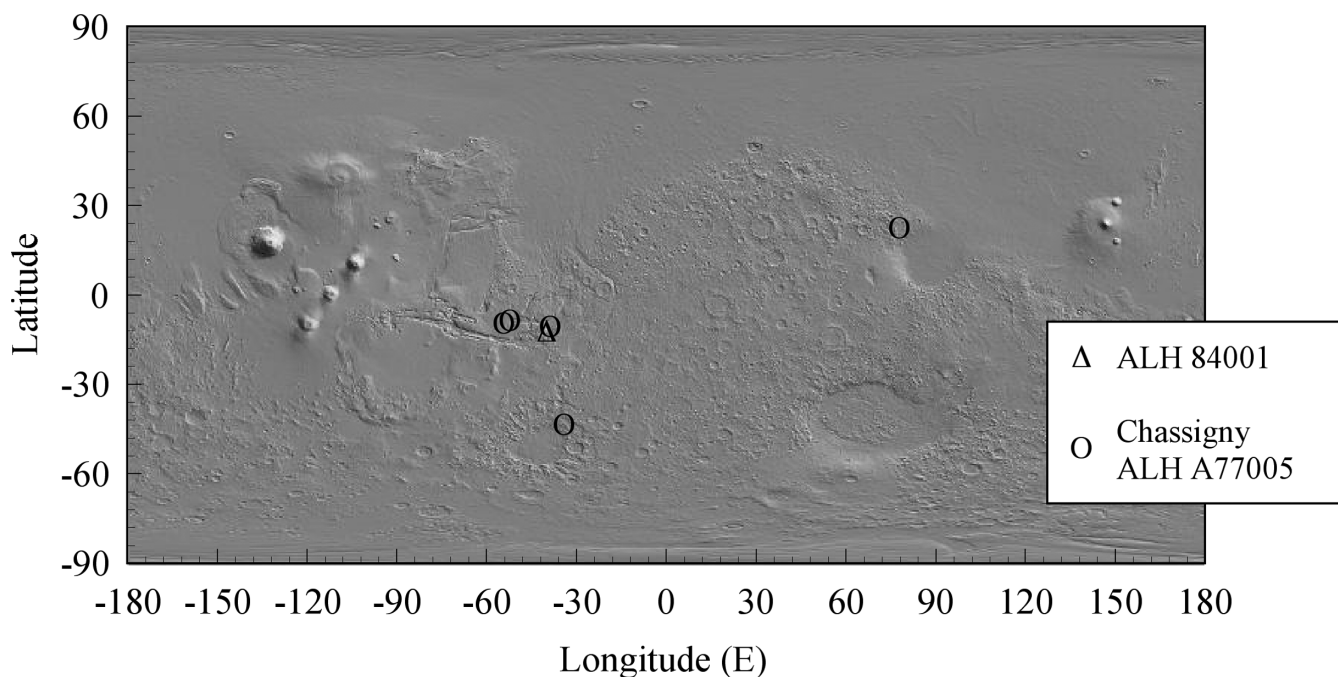
Fig. 2. Locations of major identifications of meteorite-like signatures described in this paper overlaid on MOLA 2 pixel per degree shaded relief. This map is not comprehensive. Global end member maps are available at http://www.higp.hawaii.edu/~hamilton/snc_maps.html.

material; until further work is complete, it means only that a meteorite-like mineralogy is a component of the surface material.

Chassigny and ALH A77005

Chassigny and ALH A77005 are discussed together because both are mineralogically dominated by olivine and were virtually always identified in the same geographic regions. Olivine was identified tentatively in TES data by Hoefen et al. (2000), Clark et al. (2000), and Hoefen and Clark (2001) and was suggested to be Chassigny-like in composition ($\sim Fo_{68}$) by Hamilton et al. (2001a, 2001b, 2002). Our global deconvolution maps showing the distributions and abundances of these end members display distinct similarities to the 25-micron band depth map of Hoefen et al. (2000) and Clark and Hoefen (2000).

Chassigny is dominated by olivine (~90 vol%), with minor amounts of pyroxene (augite and orthopyroxene, ~5 vol%), and feldspar (<5 vol%) (Prinz et al. 1974). ALH A77005 contains high abundances of olivine (~44–60 vol%) and pyroxene (augite and orthopyroxene, ~13–43 vol%), with maskelynite (shocked feldspar) (~10 vol%) and minor amounts of opaques and accessory phases (McSween et al. 1979; e.g., Ma et al. 1981; Mason 1981; Treiman et al. 1994). Both end members were identified in data acquired at differing times during the mission and during variable atmospheric conditions (e.g., high/low dust loading, high/low cloud cover), adding to the robustness of the identifications. The Chassigny end member was used in fits of data from Nili

Fossae near Syrtis Major (concentrations up to 0.20, Fig. 3), the southwestern portion of the Isidis rim (up to 0.12), within craters southwest of Ganges Chasma (up to 0.20), and in Ganges and Eos Chasmata (up to 0.17). Inside the northeastern Hellas basin rim, the Chassigny end member was included up to concentrations of 0.13 and on the northeastern Argyre basin rim at concentrations up to 0.16. The Isidis, Hellas, and Argyre concentrations that are above the detection limit are limited to a very few pixels at 16 pixels/degree. The spectral shape of ALH A77005 was identified in primarily the same regions as the Chassigny end member.

An example TES spectrum of an olivine-bearing surface is shown in Fig. 4. Figure 5 shows the spectrum of Chassigny compared to a ratio of TES spectra from Nili Fossae and the atmospherically corrected and modeled surface spectra. The ratio spectrum, derived by dividing spectra with and without the Chassigny-like component, clearly exhibits features consistent with olivine (as represented by Chassigny), indicating that differences in olivine abundance distinguish surface spectra in this region. Ratios (or differences) of two spectra contain contributions from both spectra and the ratio spectrum should be interpreted with caution (Ruff and Christensen 2002). Provided that other components contributing to the spectral signatures are not varying significantly or are spectrally bland over a large portion of the spectral region (e.g., basaltic and andesitic materials with few high-frequency features), recognizable features will be apparent. The atmospherically corrected surface spectrum is the most accurate representation, and in addition to olivine features, exhibits features in the 1100–1250 cm^{-1} region that,
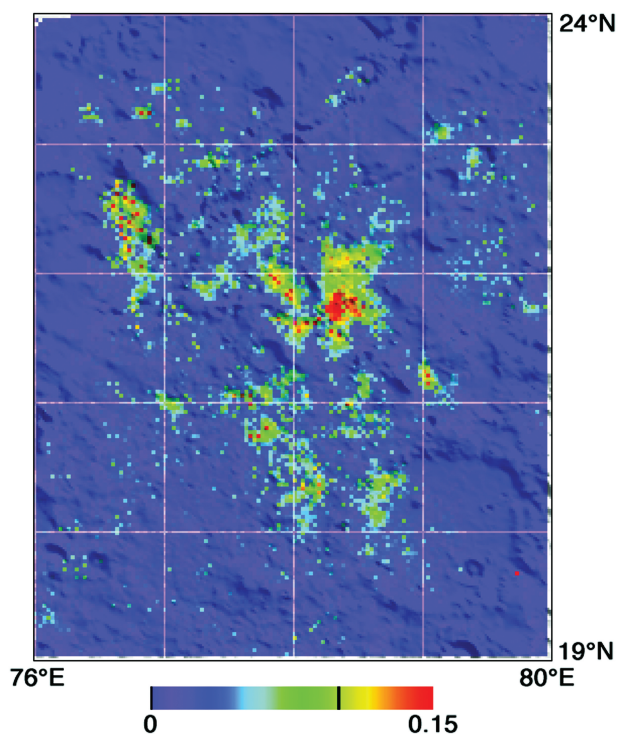
Fig. 3. Chassigny end member distribution and concentration in Nili Fossae. The vertical line in the scale bar denotes the detection limits, and the data have been interpolated to fill the map.
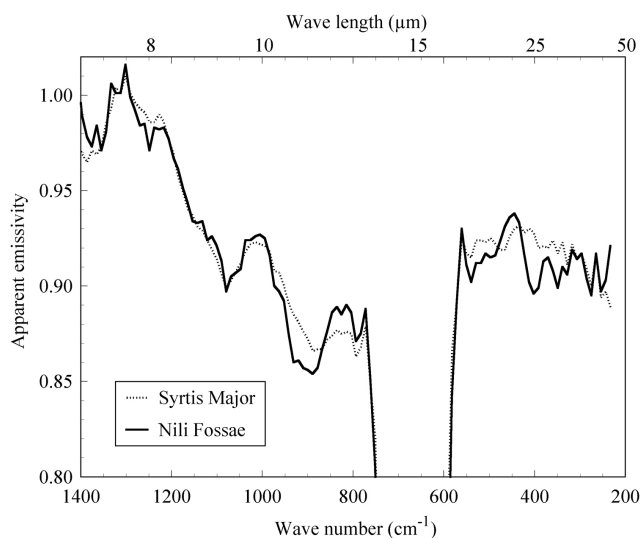

Fig. 4. Comparison of TES surface spectra from Nili Fossae (modeled with ALH A77005 and Chassigny end members) and Syrtis Major (typical martian basalt) under similar atmospheric conditions. Features in the 1200–800 cm^{-1} region dominantly are due to atmospheric dust and water ice clouds, and surface silicates dominate long wavelength features. The absorption centered at ~665 cm^{-1} is due to atmospheric CO_2. The Nili Fossae spectrum shows significant differences from a typical basaltic surface in both the 1000–800 cm^{-1} region and the 600–300 cm^{-1} region, indicating a different surface composition is present. High frequency features from 300–200 cm^{-1} are water vapor rotational modes superposed on surface absorptions (the primary cause of generally lower emissivity in this region).

are are due to a basaltic component containing feldspar and pyroxene. The composition of olivine in these meteorites is approximately Fo_{68}, and the composition on the surface must be similar because olivine absorption features vary significantly in position as a function of composition (Salisbury et al. 1991; Hamilton et al. 1997).

In spectra where either of these 2 end members was identified, one or both of the basaltic and andesitic end members was also identified. For spectra best fit using ALH A77005, the abundance of the basaltic and/or andesitic end member can be less or greater than the abundance of the meteorite end member, and surface abundances of ALH A77005-like material can exceed 70% in Nili Fossae and the Argyre rim site. For spectra best fit with the Chassigny end member, the basaltic and/or andesitic end member is always included in greater (normalized surface) abundances than Chassigny. The Chassigny end member is not included in any spectrum at abundances exceeding ~30% of the surface material. Although detection limits have been set at 0.10 or higher in this study, olivine-bearing materials are readily detected at lower concentrations in the Nili Fossae area (Fig. 3). Inspections of spectra with detections <0.10 show that olivine spectral features are visible. Laboratory deconvolution experiments have shown that detection limits vary with the mineral (Feely and Christensen 1997; Wyatt et al. 2001); olivine has particularly strong and, in some cases, narrow features that readily distinguish it from many other minerals, and our results suggest that detection limits for olivine may be substantially lower (~0.05) than 0.10.

Although the Chassigny and ALH A77005 end members commonly were identified in the same geographic location—which is not surprising because both meteorites are dominated by olivine—they are rarely identified in the same pixel, and no spectra were identified in which the surface component is modeled exclusively with either end member. This result implies that these surfaces may be physical mixtures of more than one lithology or exhibit a previously unidentified lithology. If the TES spectra represent a mixed signal from distinct subpixel-sized areas, e.g., basaltic and Chassigny-like surfaces, we would interpret the TES spectra as representing 2 distinct lithologies, one of which has high potential for being a meteorite source material. If, on the other hand, the materials represent a new lithology, we might interpret these surfaces as being basaltic materials that entrained and erupted olivine-rich xenoliths—a material with a very different geologic interpretation. A more detailed understanding of the bulk mineralogy will be obtained in future deconvolutions of TES data that use mineral end members exclusively, and comparisons of mineralogy as a function of location, topography, etc., may help distinguish between lithologic variations and mixtures. In the meantime, high spatial resolution imaging data from the Mars Orbiter Camera (MOC), where available, can help address the nature of these surfaces. MOC images over Nili Fossae show geologically complex surfaces that will require significant
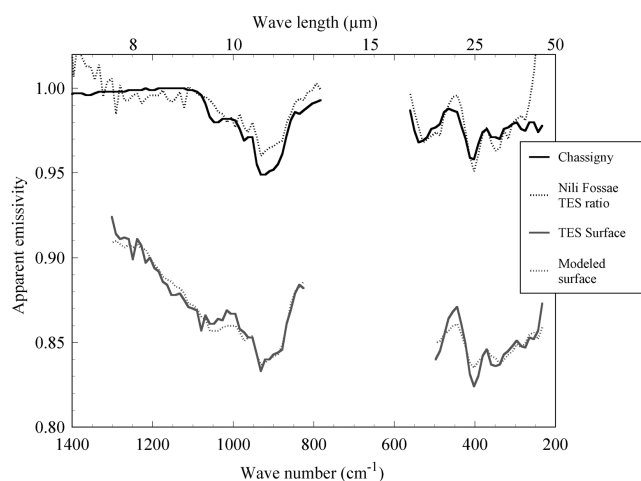
Fig. 5. Comparison of TES spectra from Nili Fossae to Chassigny spectrum. The laboratory spectrum of Chassigny is shown at 20% of its spectral contrast for comparison and the ratio spectrum is contrast enhanced to 150% for visibility; all others are shown at full spectral contrast. The region of atmospheric CO_2 absorption is excluded from all spectra; the TES and modeled surface spectra exclude a greater portion of the atmospheric region to ensure that no atmospheric component affects the model. For clarity, the TES and modeled surface spectra are offset vertically by –0.10.

effort to interpret. Figure 6 shows an example of terrain in Nili Fossae associated with the highest abundances of the Chassigny end member (Fig. 3). This image shows a tortured surface exhibiting layering, evidence of aeolian processes, surfaces of varying relative albedo, and ridges that might represent igneous dikes or contraction features. This image suggests clearly that more than one lithology is present in this region but that physical mixing of these materials is making their distinction at TES scales difficult. Thermal inertias of the highest concentration olivine-bearing materials range from 450–650 J m^{-2}K^{-1}s$^{-1/2}$ throughout Nili Fossae, suggesting that they have average properties of very coarse materials and may even consist of bedrock overlain, in some areas, by sands.

At the 16 pixel/degree scale of this study, there are 2 locations with compelling correlations between the occurrence of meteorite-like lithologies and craters of appropriate dimensions such that they might be parent craters. The first correlation is present where olivine-dominated meteorites (Chassigny and ALH A77005) are identified in 2 craters southwest of Ganges Chasma. Olivine-bearing spectral signatures are identified in the western interior deposits of these craters but are not identified in the outer rim and what remains of the ejecta blanket materials. The thermal inertias of these deposits are high (~450–650 J m^{-2}K^{-1}s$^{-1/2}$) and suggest that the materials in these craters are extremely coarse or rocky particulates, indurated/lithified sediments, or possibly even partly exposed bedrock. These craters are located in Noachian terrain, which is much older than either the 1.3 Gyr age of Chassigny or the 0.18 Gyr age of
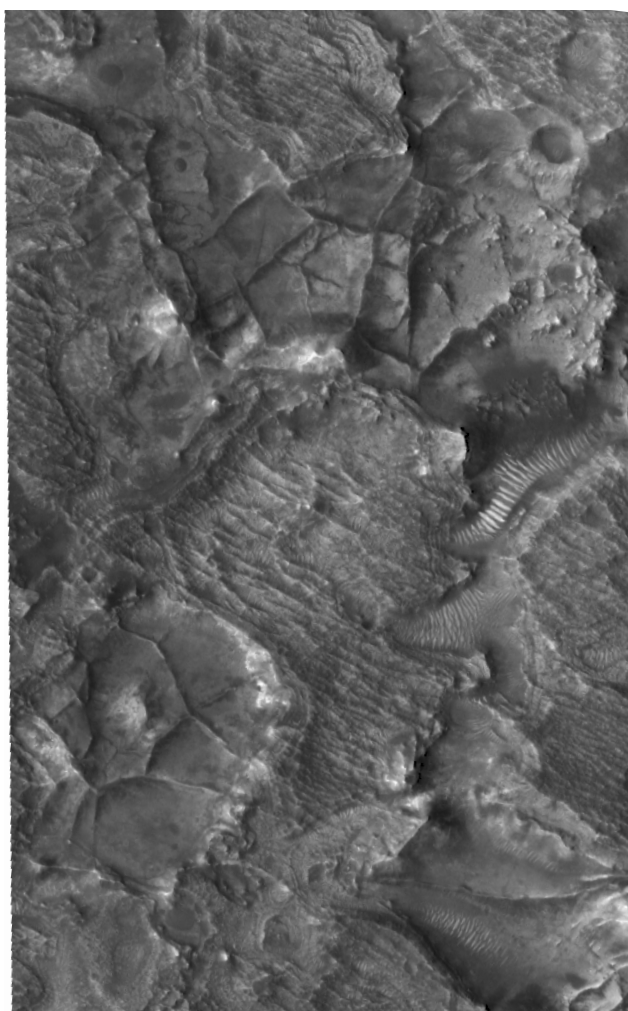

Fig. 6. Portion of MOC image E05–00782, centered at approximately 22°N, 77°E, showing olivine-bearing terrain in Nili Fossae (image is ~3 km wide). Terrain in this region is etched in appearance, with numerous layered deposits, dune forms, and intersecting ridges. Igneous and/or sedimentary origins for the layering and ridges are possible.

ALH A77005, reducing the likelihood that these are parent craters for either meteorite. The true age and origin of the materials that fill these craters are very poorly understood.

Occurrences of Chassigny- and ALH A77005-like signatures in Nili Fossae are spread over a region large enough to contain a number of craters with the requisite dimensions to be considered candidates, so spatial correlations and mapping at higher resolution than is presented here will be necessary to identify all potential source craters. One piece of evidence that tends to indicate that Nili Fossae is not a good candidate source region for either meteorite is the apparent ancient age of the surface (Noachian). However, high resolution imaging of portions of Mars are revealing much younger terrains (within older terrains) than previously known (Hartmann 1999; Hartmann and Berman 2000); detailed MOC and THEMIS images might help establish whether or not olivine-bearing materials

in Nili Fossae are younger than the region as a whole. Another criterion that might be used to identify regions or individual craters with greater probabilities of being meteorite sources is the presence of paired lithologies— meteorites that show evidence in their cosmic ray exposure (CRE) ages of having been ejected simultaneously. Chassigny and ALH A77005 are not closely related nor of the same age, but Chassigny and Nakhla are (Nyquist et al. 2001). Thus, a Chassigny source region might be expected to contain Nakhla-like signatures as well. Nakhla-like mineralogy is not identified at or above the detection limit in the Nili Fossae region, which may ultimately indicate that Nili Fossae, although rich in olivine-bearing materials, is not the source region for Chassigny (or the nakhlites). However, Nili Fossae as a potential source region for ALH A77005 is not ruled out.

The unequivocal identification of olivine (whether or not it can be linked to a martian meteorite) is of interest because its presence can be used to draw some broad inferences about the rate of chemical weathering of the martian surface since the time these materials crystallized. Of the primary silicate minerals, olivine is the most susceptible to chemical breakdown. The TES spectra are modeled well with lithologic end members that contain volumetrically high abundances of olivine and/or low abundances of weathering/alteration products. However, these terrains have estimated absolute ages of over 3 Gyr (regardless of cratering chronology used), suggesting that chemical alteration of the surface and shallow subsurface has been occurring at very low rates over most of Mars' geologic history (barring evidence that these materials erupted significantly more recently).

Nakhla

Nakhla stones vary in their modal mineralogy, but are dominated by high-Ca clinopyroxene (augite, ~80 vol%) with olivine (~5–18 vol%, varies inversely with augite abundance [Friedman Lentz et al. 1999]), plagioclase feldspar (~4 vol%), and minor (~2 vol%) accessory phases (Berkley et al. 1980). In our examination of all spectra with concentrations of the Nakhla end member exceeding the minimum detection limit, we retrieved a large number (thousands) that do not display any obvious spatial coherence. A plot of when these spectra were acquired (orbit number, OCK) versus latitude shows that their occurrence is primarily restricted to data collected subsequent to ~OCK 7000 and is correlated with sub-solar latitude (this figure is available at http://www.higp.hawaii.edu/~hamilton/snc_maps.html).

Bandfield (2002) noted, but did not describe in detail, an "anomaly" in TES data beyond OCK 7000 that is manifested as the introduction of a minor feature in spectral data at ~1000 cm^{-1}. This feature is introduced randomly over a series of sequential ICKs (the 2 seconds during which spectra are acquired) but occurs simultaneously in all 6 detectors of a given ICK and may be a positive or negative feature. Analysis

by the TES team has determined that this spectral anomaly is the manifestation of microphonic noise induced by vibration of the aging MGS spacecraft. The occurrence of this noise in the spectral data has been mapped by the TES team (M. D. Smith, personal communication) and closely matches the plot of Nakhla identifications in time and latitude, suggesting that the vast majority of Nakhla identifications after ~OCK 7000 are spurious. Because Nakhla is dominated by clinopyroxene, which has an emission maximum near 1000 cm^{-1}, it is likely included in the best fit of spectra where the anomalous feature is positive (an emission maximum). The presence of this feature and the likelihood of its being mapped as compositional information suggest that care should be exercised in the use of individual ICKs and pixels acquired after OCK 7000 in compositional studies. The spectral anomaly is randomly a positive or negative feature of variable amplitude, and local to regional averages of spectra post-OCK 7000 may used for compositional studies because they average out the anomaly. But, particular caution should be used when attempting to study variations in any mineral with a strong emission minimum or maximum near 1000 cm^{-1}. The noise anomaly only affects data from the TES interferometer; this issue does not affect data from the visible and thermal bolometers. For many purposes, such as water vapor retrievals and studies of cold surfaces that generally use only spectral data at wavelengths >20 μm, the spectral data are unaffected.

For the remainder of our discussion of the Nakhla end member, we have excluded results from data acquired post-OCK 7000. In the pre-OCK 7000 data, a Nakhla-like spectral shape was identified at low concentrations (≤~0.10) in several regions, most notably in the eastern Valles Marineris region, in Juventae, Capri, and Eos chasmata, and in some craters in the outlying plains. Other locations where this end member was used at or above the detection limit include localized areas within the broader Terra Tyrrhena region and in the regions surrounding Nili and Meroe Patera in Syrtis Major Planum. Although most of these identifications are near the detection limit, their spatial distribution is non-random, suggesting that, as in the case of olivine, they may be valid, but further work is required to confirm them.

If valid, the observed distribution of Nakhla-like material may represent variations in the clinopyroxene content of the local lithology(ies) rather than the presence of nakhlite-like materials, but this distinction cannot be made at the scale of the present study. Broad regional surfaces that are modeled with the Nakhla end member typically are correlated with the basaltic end member rather than the intermediate end member, which may support the interpretation that these detections are variations in pyroxene content within basalt.

At the scales examined here, the identification of Nakhla-like material near the detection limit in broad regions, rather than as concentrated deposits, does not point to a single, specific candidate site for the nakhlites. As described above, nakhlite compositions are not obviously associated with

elevated olivine abundances as might be expected if the nakhlites and Chassigny shared a common source region. Higher-resolution studies of spatially restricted areas in Syrtis Major with moderately strong clinopyroxene signatures may reveal potential source terrains.

ALH 84001

ALH 84001 is composed almost entirely (~97 vol%) of orthopyroxene (Mason et al. 1992). A small region (~625 km²) in Eos Chasma was identified as having a spectral component like the ALH 84001 end member (Fig. 7), with concentrations up to 0.40 and normalized surface abundances up to ~45%. As in the cases of Chassigny and ALH A77005, the ALH 84001-like signature was identified in this area repeatedly throughout the nominal mission in data acquired during seasons with variable atmospheric conditions. No other spatially significant sites have been identified at the 16 pixel/degree scale, although numerous single- to few-pixel identifications exist, particularly in the Valles Marineris floor.

Because this is a new mineral identification, we were particularly rigorous in confirming the deconvolution result, and we used several approaches to manually inspect spectra that were modeled with high concentrations of the ALH 84001 end member. First, comparison of Eos Chasma spectra having high concentrations of the ALH 84001 end member with spectra from a typical basaltic region (Syrtis Major) display notable differences at long wavelengths (Fig. 8), which is indicative of differing compositions. Next, we compared spectra with ALH 84001-like spectral components to spectra in the same orbit having little or no detectable amount of the relevant end member by ratioing them. Ratios
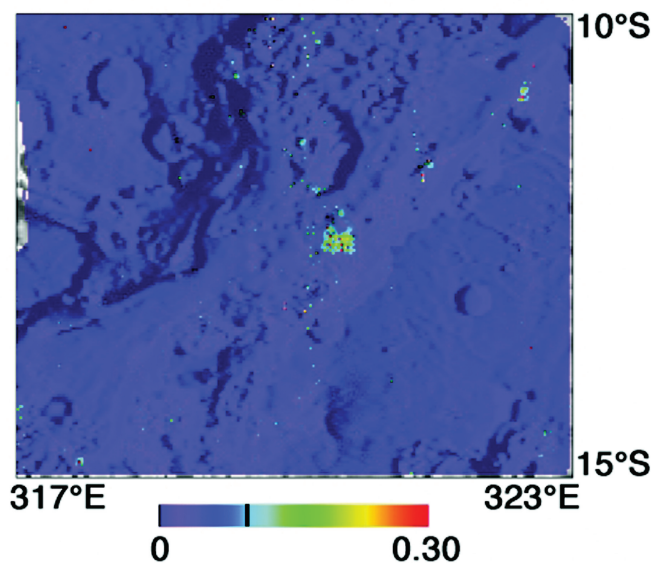

Fig. 7. ALH 84001 end member distribution and concentration in Eos Chasma. The vertical line in the scale bar denotes detection limits, and the data have been interpolated to fill the map.

of spectra from multiple orbits in Eos Chasma consistently display features that are remarkably similar to the spectrum of ALH 84001 (Fig. 9). Finally, we removed the spectral contribution of the atmospheric components, showing the surface spectrum's strong resemblance to that of the orthopyroxenite (Fig. 9). ALH 84001 is not the sole component of any of the Eos Chasma spectra, so subtle differences between the ALH 84001 spectrum and the atmospherically corrected Eos Chasma spectrum result in part from a basaltic component that is present in the Eos spectra.

The identification of an ALH 84001-like signature in this study provides the first unambiguous detection of orthopyroxene on the martian surface. The geographic association of this material with knobs and canyon walls suggests that it may be the debris of an in situ outcrop. Thermal inertias in this area range from 200–730 J m^{-2}K^{-1}s$^{-1/2}$ and indicate that the physical character of surface materials probably spans a range from fine sands to coarse sands and/or a high density of rocks. This material is associated with young Valles Marineris floor materials, which appear to be inconsistent with an ALH 84001 source region, considering the meteorite's ancient age. On the other hand, the floor materials possibly are sediments eroded from nearby in situ deposits or otherwise exposed by erosion of overlying units. This idea is consistent with the exposure of igneous rocks in the basal wall rocks of the Valles Marineris at elevations ~4 km below datum. Unfortunately, no high-resolution Viking or MOC images have been acquired in this area to help clarify the nature of the deposit. As in the case of the detection of olivine, the presence of orthopyroxene on the martian surface has some interesting implications. Pyroxenes also tend to be susceptible to weathering and alteration, and the presence of significant quantities of orthopyroxene on the martian surface suggests again that on large scales, rates of weathering at the martian surface are relatively slow.

Promising source regions for ALH 84001 also remain elusive. The ancient age of the meteorite (~4.5 Gyr) strongly suggests that it must have come from what should be a highly cratered terrain. Considering the relatively small number of martian meteorites identified, the fact that one is this old may indicate that it represents a widespread material. However, only one spatially significant region (Eos Chasma) was identified as having a strong orthopyroxene signature; if this material is mechanically weathered out of the lower layers of the Valles Marineris, it could be of the appropriate age, but no obvious candidate crater is nearby. ALH 84001 exhibits evidence for having experienced more than one shock event, the first of which is interpreted to represent an early impact that brought the rock near enough to the surface to be ejected in a later event (Nyquist et al. 2001). This complicated history may mean that regardless of its global abundance, the ALH 84001 orthopyroxenite/source region is not widely exposed at the optical surface of Mars, but is instead a small area exposed by impact gardening.

Zagami and Los Angeles

Zagami and Los Angeles are discussed together because both are shergottites. Zagami is a basaltic shergottite composed of ~75–80 vol% pyroxene (~equal amounts of augite and pigeonite), ~10–20 vol% maskelynite, and ~5 vol% mesostasis and minor phases (Stolper and McSween 1979; McCoy et al. 1992). Detectable abundances of Zagami-like mineralogy are located in only a very few pixels, predominantly within the Terra Tyrrhena region. These detections are not spatially significant and require further work for confirmation; thus, they are not considered further in this study.

Los Angeles was included as an end member in this study because it differs considerably in mineralogy and mid-IR spectral character from other shergottites (Hamilton et al. 2001b). Los Angeles (stone 1) is composed of ~44–45 vol% maskelynite and ~38–44 vol% pyroxene, with the remainder consisting of small amounts of silica, oxides, olivine, glass, and other phases (~2–5 vol% each) (Rubin et al. 2000). Concentrations of the Los Angeles end member are typically below the 0.10 detection limit, and its distribution is highly correlated with surfaces having albedos of 0.20–0.24, which are at the high end for the data analyzed in this study. Manual inspection of the spectra from areas where the Los Angeles end member was included in the model fits shows that these spectra are characterized by decreased emissivity at short wavelengths, which is characteristic of fine particulate materials. Therefore, we conclude that the distribution and spatial coherence of the Los Angeles end member identifications indicates that some characteristic of those spectra differs from other spectra on Mars, but we are not convinced that it is due to the presence of a Los Angeles-like lithology. As a result of the finer nature of these particulate surfaces, these spectra are less reliably modeled by the coarse particulate to solid sample spectral end members used in this study and require further examination to determine the cause of the meteorite end member identification. Other identifications of this end member were not spatially significant and are not considered further.

Our data demonstrate that shergottite lithologies do not provide good matches to the mineralogy of martian dark regions. One might question whether the use of basaltic shergottite lithologies other than the two used here (e.g., olivine-phyric/picritic shergottites) would produce a different result. Although some variability exists among the basaltic shergottites, they all have mineralogies that are similar enough to confidently classify them unambiguously as a distinctive group that would be distinguishable from the TES-derived basaltic lithology. At the spectral resolution and SNR of the TES instrument, these relatively subtle differences are unlikely to be distinctive enough such that the spectrum of Zagami, Los Angeles, or (for example) a combination of Zagami and ALH A77005 would be incapable of locating them. The geologically young ages of the shergottites have
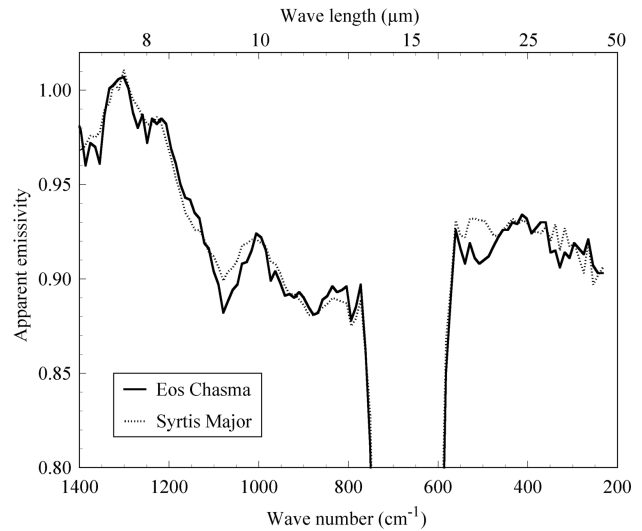

Fig. 8. Spectrum of material in Eos Chasma compared to typical basaltic surface spectrum from Syrtis Major under similar atmospheric conditions. The 1200–800 cm^{-1} region is dominated by spectral features of silicate dust and water ice clouds in the atmosphere, although features due to surface components also are present. The absorption centered at ~665 cm^{-1} is due to atmospheric CO_2. The two spectra display significant variations in the 550–200 cm^{-1} region (particularly near 500 cm^{-1}) resulting from differences in surface component composition. The high frequency features at longer wavelengths are water vapor rotational bands.
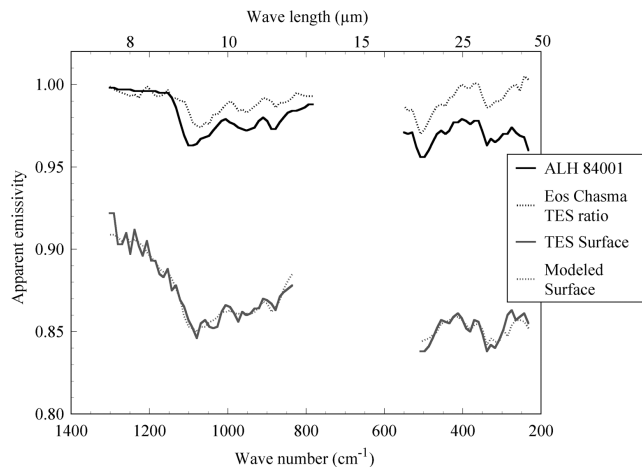

Fig. 9. Comparison of TES spectra from Eos Chasma to ALH 84001 spectrum. The spectrum of ALH 84001 is shown at 40% spectral contrast; all others are shown at full spectral contrast. The region of atmospheric CO_2 absorption is excluded from all spectra; the TES and modeled surface spectra exclude a greater portion of the atmospheric region to ensure that no atmospheric component affects the model. For clarity, the TES and modeled surface spectra are offset vertically by −0.10.

been cited as evidence that their sources may lie in geologically young terrains such as Tharsis, Elysium, and/or Amazonis (Mouginis-Mark et al. 1992; Nyquist et al. 2001; McSween 2002). Unfortunately, optically thick layers of dust

cover these young igneous terrains. Mineralogical remote sensing instruments cannot penetrate dust-covered surfaces to determine the underlying mineralogy and so cannot be used to address the question of whether or not shergottites are present in these areas. Future landed or sample return missions with the capability to retrieve rocky materials from underneath centimeters to meters of dust cover will be our best opportunity to determine the mineralogy of Mars' youngest igneous provinces and their possible relationship to the martian meteorites.

INTEGRATING MARTIAN METEORITES AND MARTIAN GEOLOGY

Having presented our analysis and interpretation of the TES data, we can now place our results into the broad picture of martian igneous and geologic processes. In doing so, we assume that the dark surfaces studied here represent the bulk mineralogy of the local crustal rocks based on the nature of the surface materials. For our purposes, we assume that the penetration depth of the remote sensing measurement is roughly equivalent to 10 times the wavelength of observation. Martian dark surfaces are dominated by mobile, coarse (~100s μm), sandy materials (e.g., Christensen and Moore 1992), and less commonly, bedrock units, so remote sensing measurements seldom represent direct measurements of crustal outcrops. However, because sand grains can travel only a limited distance from their source (tens to hundreds of km [White 1979; Greeley and Kraft 2001]) without becoming comminuted to grain sizes that will be blown away, we can reasonably assume they are locally derived where present.

Initially, our results seem inconsistent with the spectroscopic observations of Mustard et al. (1993), Mustard and Sunshine (1995), and Mustard et al. (1997), who found that visible to near infrared (VNIR) spectra of martian dark regions appeared to be consistent with the widespread presence of shergottite-like lithologies. However, VNIR and thermal IR measurements can be used together to place constraints on each other and on the martian surface composition, and we believe the ISM and TES data can be reconciled. In the case of the martian VNIR spectra from ISM, Fe-related band positions and shapes were used to identify high- and low-Ca pyroxene and determine their relative abundances. These relative abundances, although consistent with the relative abundances of high- and low-Ca pyroxene in shergottites, are also consistent with a wide range of absolute abundances that may differ significantly from those in shergottites. When the modal mineralogy of major phases in martian dark regions is modeled using TES data, plagioclase, not pyroxene, is seen as the dominant phase. However, the relative abundances of pyroxenes derived from ISM are similar to TES abundances; the modal mineralogy of the basaltic surface type identified in TES data (as typified by the spectra of Syrtis Major) includes ~25 vol% high-Ca pyroxene and ~5 vol% orthopyroxene (which is below TES

detectability limits). This is a high- to low-Ca pyroxene ratio of 5:1, which is similar to the ratio derived from the ISM data (4:1) of Syrtis Major (Mustard et al. 1997; Mustard, personal communication). In terms of composition, the TES basaltic spectrum is fit well using high-Ca augite and orthopyroxene; at the abundances required by shergottite compositions, low-Ca augite and pigeonite (as actually found in the shergottites) would not fit the spectra well. The pyroxene 1- and 2-μm band positions derived from the ISM spectra were not discussed in detail by Mustard et al. (1997) but are consistent with the band positions of high-Ca clinopyroxenes and orthopyroxenes (Fig. 10) measured in laboratory studies (Adams 1974; Cloutis and Gaffey 1991).

The lack of pyroxene-dominant basalts in martian dark regions implies that the martian crust is dominated by a basalt having "normal" Al content. We suggest that the extraction of this crustal component, with melting of garnet in the mantle (Longhi et al. 1992), is likely the event that depleted the martian mantle in Al. The mean martian crustal thickness is about 50 km, which is a significant fraction of Mars' volume (4%; Zuber et al. 2000) and represents a significant amount of volcanism that could produce a depleted mantle.

So what do the martian meteorites represent? Our work supports the previously proposed idea that the meteorites (except ALH 84001) are a biased sampling of the youngest martian crust. Terrains having ages most consistent with the ages of the shergottites include Tharsis, Amazonis, and Elysium (e.g., Nyquist et al. 2001). Unfortunately, even if shergottite or other meteorite lithologies are exposed on these surfaces, they are likely to be hidden from mineralogical remote sensing instruments by the pervasive dust that covers these regions (Christensen and Moore 1992; Mellon et al. 2000).

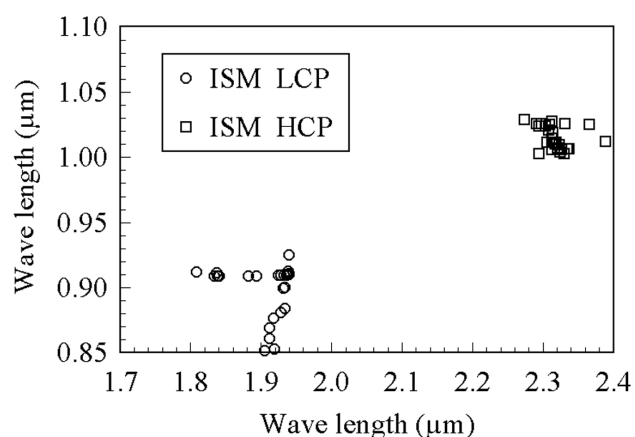Soils at the Viking and Pathfinder landing sites appear to

Fig. 10. Modeled positions of pyroxene 1- and 2-μm bands in the Phobos 2 ISM data of Mars from Table 2 of Mustard et al. (1997). The positions are consistent with orthopyroxene and high-Ca clinopyroxene. The uncertainties in the modeled band positions are ~20–30 nm; points below ~0.89 likely reflect contamination by Fe^{3+} (Mustard, personal communication).

be Al-depleted and have been interpreted as having been derived from Al-depleted materials (McSween and Keil 2000), which seems inconsistent with weathering from a plagioclase-dominant basaltic crust. One explanation for this disparity might relate to the timing and/or rate of soil development. Volcanism at Tharsis and Elysium was voluminous and active into Mars' relatively recent geologic history. If this volcanism produced the Al-depleted shergottites, then perhaps the dust and soils measured in situ have developed relatively recently in Mars' history from the products of this volcanism and have been transported globally by seasonal storms (after weathering) or by the volcanism itself (with subsequent in situ weathering). A recent geomorphology study by Mouginis-Mark (2002) provides evidence for explosive volcanism among these volcanoes, which could provide a means of dispersing Al-depleted materials across much of the planet over time. If the composition of crustal materials has evolved over time, then we may reasonably suggest that global soil compositions derived from crustal material have evolved similarly over time and that recent soils may bury older, less Al-depleted soils.

CONCLUSIONS

1. The majority of dark surfaces on Mars generally are not well matched by martian meteorite spectra, suggesting that martian meteorite chemistries are not representative of a large fraction of the martian crust. The dominance of previously identified plagioclase-rich basaltic compositions suggests that the bulk of the martian crust is not Al depleted.

2. Olivine-bearing materials resembling ALH A77005 and Chassigny were identified in localized areas of ancient terrains inconsistent with the ages of these meteorites.

3. The identification of orthopyroxene-bearing material in Eos Chasma is the first positive identification of orthopyroxene on Mars. If this material is a candidate source region for ALH 84001, its presence in Eos Chasma is inconsistent with the ancient age of that meteorite unless this material is derived from mechanical weathering of in situ outcrops or the canyon walls and is older than the valley floor materials.

4. Significant concentrations (>0.10–0.15) of basaltic shergottite-like materials have not been identified at the spatial scales considered in this study. These meteorites have cumulate textures and compositions that imply that their parent materials may not be widely distributed on the uppermost surface (i.e., top tens to hundreds of microns), even if they reside within the upper few meters of the surface, and may explain their virtual absence in spectroscopic data.

5. The ultramafic lithologies like Chassigny, ALH A77005, and ALH 84001 observed in TES data appear relatively

unweathered for their presumed age. This seeming contradiction may suggest that rates of chemical weathering in the uppermost martian crust are very slow or that more recent volcanism has occurred within older terrains.

Editorial Handling—Dr. Allan Treiman

REFERENCES

Adams J. B. 1974. Visible and near-infrared diffuse reflectance spectra of pyroxenes as applied to remote sensing of solid objects in the solar system. *Journal of Geophysical Research* 79:4829–4836.

Adams J. B. and McCord T. B. 1969. Mars: Interpretation of spectral reflectivity of light and dark regions. *Journal of Geophysical Research* 74:4851–4856.

Bandfield J. L. 2002. Global mineral distributions on Mars. *Journal of Geophysical Research* 107(E6), doi: 10.1029/2011JE001510.

Bandfield J. L., Hamilton V. E., and Christensen P. R. 2000. A global view of martian surface compositions from MGS-TES. *Science* 287:1626–1630.

Barlow N. G. 1997. The search for possible source craters for martian meteorite ALH 84001 (abstract #1661). 28th Lunar and Planetary Science Conference. CD-ROM.

Berkley J. L., Keil K. and Prinz M. 1980. Comparative petrology and origin of Governador Valadares and other nakhlites. Proceedings, 11th Lunar and Planetary Science Conference. pp. 1089–1102.

Bibring J. P., Combes M., Langevin Y., Cara C., Drossart P., Encrenaz T., Erard S., Forni O., Gondet B., Ksanfomality L., Lellouch E., Masson P., Moroz V., Rocard F., Rosenqvist J., Sotin C., and Soufflot A. 1990. ISM observations of Mars and Phobos: First results. Proceedings, 20th Lunar and Planetary Science Conference. pp. 461–471.

Bogard D. D., Nyquist L. E., and Johnson P. 1984. Noble gas contents

of Shergottites and implications for the martian origin of SNC meteorites. *Geochimica et Cosmochimica Acta* 48:1723–1739.

Christensen P. R., Anderson D. L., Chase S. C., Clark R. N., Kieffer H. H., Malin M. C., Pearl J. C., Carpenter J., Bandeira N., Brown F. G., and Silverman S. 1992. Thermal emission spectrometer experiment: The Mars Observer Mission. *Journal of Geophysical Research* 97:7719–7734.

Christensen P. R., Bandfield J. L., Clark R. N., Edgett K. S., Hamilton V. E., Hoefen T., Kieffer H. H., Kuzmin R. O., Lane M. D., Malin M. C., Morris R. V., Pearl J. C., Pearson R., Roush T. L., Ruff S. W., and Smith M. D. 2000a. Detection of crystalline hematite mineralization on Mars by the thermal emission spectrometer: Evidence for near-surface water. *Journal of Geophysical Research* 105:9623–9642.

Christensen P. R., Bandfield J. L., Hamilton V. E., Ruff S. W., Kieffer H. H., Titus T. N., Malin M. C., Morris R. V., Lane M. D., Clark R. N., Jakosky B. M., Mellon M. T., Pearl J. C., Conrath B. J., Smith M. D., Clancy R. T., Kuzmin R. O., Roush T. L., Mehall G. L., Gorelick N., Bender K., Murray K., Dason S., Greene E., Silverman S., and Greenfield M. 2001a. Mars Global Surveyor thermal emission spectrometer experiment: Investigation description and surface science results. *Journal of Geophysical Research* 106:23823–23871.

Christensen P. R., Bandfield J. L., Smith M. D., Hamilton V. E., and Clark R. N. 2000b. Identification of a basaltic component on the martian surface from thermal emission spectrometer data. *Journal of Geophysical Research* 105:9609–9621.

Christensen P. R. and Harrison S. T. 1993. Thermal infrared emission spectroscopy of natural surfaces: Application to desert varnish coatings on rocks. *Journal of Geophysical Research* 98:19819–19834.

Christensen P. R., Kieffer H. H., Chase S. C., and LaPorte D. D. 1986. A thermal emission spectrometer for identification of surface composition from Earth orbit. In *Commercial applications and scientific research requirements for thermal-infrared observation of terrestrial surfaces.* Washington: National Aeronautics and Space Administration. pp. 119–132.

Christensen P. R. and Moore H. J. 1992. The martian surface layer. In *Mars,* edited by Kieffer H. H., Jakosky B. M., Snyder C. W., and Matthews M. S. Tucson: University of Arizona Press. pp. 686–729.

Christensen P. R., Morris R. V., Lane M. D., Bandfield J. L., and Malin M. C. 2001b. Global mapping of martian hematite mineral deposits: Remnants of water-driven processes on early Mars. *Journal of Geophysical Research* 106:23873–23885.

Clark R. N. and Hoefen T. M. 2000. Spectral feature mapping with Mars Global Surveyor thermal emission spectra: Mineral implications (abstract). *Bulletin of the American Astronomical Society* 32:1118.

Cloutis E. A. and Gaffey M. J. 1991. Pyroxene spectroscopy revisited: Spectral-compositional correlations and relationships to geothermometry. *Journal of Geophysical Research* 96:22809–22826.

Crown D. A. and Pieters C. M. 1987. Spectral properties of plagioclase and pyroxene mixtures and the interpretation of lunar soil spectra. *Icarus* 72:492–506.

Eugster O., Weigel A., and Polnau E. 1997. Ejection times of martian meteorites. *Geochimica et Cosmochimica Acta* 61:2749–2757.

Feely K. C. and Christensen P. R. 1997. Modal abundances of rocks using infrared emission spectroscopy. 28th Lunar and Planetary Science Conference. pp. 349–350.

Feely K. C. and Christensen P. R. 1999. Quantitative compositional analysis using thermal emission spectroscopy: Application to igneous and metamorphic rocks. *Journal of Geophysical Research* 104:24195–24210.

Friedman Lentz R. C., Taylor G. J., and Treiman A. H. 1999. Formation of a martian pyroxenite: A comparative study of the nakhlite meteorites and Theo's Flow. *Meteoritics & Planetary Science* 34:919–932.

Gladman B. J. 1997. Destination: Earth. Martian meteorite delivery. *Icarus* 130:228–246.

Greeley R. and Kraft M. 2001. Survivability of aggregate sands on Mars (abstract #1839). 32nd Lunar and Planetary Science Conference. CD-ROM.

Hamilton V. E. and Christensen P. R. 2000. Determining the modal mineralogy of mafic and ultramafic igneous rocks using thermal emission spectroscopy. *Journal of Geophysical Research* 105:9717–9733.

Hamilton V. E., Christensen P. R., and McSween H. Y., Jr. 2002. Global constraints on the source regions of martian meteorites from MGS TES data. *Meteoritics & Planetary Science* 37:A59.

Hamilton V. E., Christensen P. R., and McSween H. Y., Jr. 1997. Determination of martian meteorite lithologies and mineralogies using vibrational spectroscopy. *Journal of Geophysical Research* 102:25593–25603.

Hamilton V. E., Christensen P. R., McSween H. Y., Jr., Clark R. N., and Hoefen T. M. 2001a. Spectral variations. In *MGS TES data of Nili Fossae: A possible source region for SNC meteorites on Mars?* (abstract #2184). 32nd Lunar and Planetary Science Conference. CD-ROM.

Hamilton V. E., McSween H. Y., Jr., and Christensen P. R. 2001b. Searching for martian meteorite source regions using Mars Global Surveyor thermal emission spectrometer (MGS TES) data. *Meteoritics & Planetary Science* 36:A75.

Hamilton V. E., Wyatt M. B., McSween H. Y., Jr., and Christensen P. R. 2001c. Analysis of terrestrial and martian volcanic compositions using thermal emission spectroscopy: II. Application to martian surface spectra from MGS TES. *Journal of Geophysical Research* 106:14733–14746.

Hartmann W. K. 1999. Martian cratering VI: Crater count isochrons and evidence for recent volcanism from Mars Global Surveyor. *Meteoritics & Planetary Science* 34:167–177.

Hartmann W. K. and Berman D. C. 2000. Elysium Planitia lava flows: Crater count chronology and geological implications. *Journal of Geophysical Research* 105:15011–15025.

Head J. N. 1999. Fragmentation and ejection of the martian clan meteorites. Ph.D. thesis, University of Arizona, Tucson, Arizona.

Head J. N. and Melosh H. J. 2000. Launch velocity distribution of the martian clan meteorites (abstract #1937). 31st Lunar and Planetary Science Conference. CD-ROM.

Head J. N., Melosh H. J., and Ivanov B. A. 2002. Martian meteorite launch: High-speed ejecta from small craters. *Science* 298:1752–1756.

Hoefen T. M. and Clark R. N. 2001. Compositional variability of martian olivines using Mars Global Surveyor thermal emission spectra (abstract #2049). 32nd Lunar and Planetary Science. CD-ROM.

Hoefen T. M., Clark R. N., Pearl J. C., and Smith M. D. 2000. Unique spectral features in Mars Global Surveyor thermal emission spectra: Implications for surface mineralogy in Nili Fossae (abstract). *Bulletin of the American Astronomical Society* 32:1118.

Jones J. H. 1985. The youngest meteorites: III. Implications of 180 m.y. igneous activity on the SPB. 32nd Lunar and Planetary Science Conference. pp. 408–409.

Jones J. H. 1986. A discussion of isotopic systematics and mineral zoning in the Shergottites: Evidence for a 180 Myr igneous crystallization age. *Geochimica et Cosmochimica Acta* 50:969–977.

Longhi J., Knittle E., Holloway J. R., and Wänke H. 1992. The bulk

composition, mineralogy, and internal structure of Mars. In *Mars,* edited by Kieffer H. H., Jakosky B. M., Snyder C. W., and Matthews M. S. Tucson: University of Arizona Press. pp. 184–208.

Lyon R. J. P. 1965. Analysis of rocks by spectral infrared emission (8–25 microns). *Economic Geology* 60:715–736.

Ma M. S., Laul J. C., and Schmitt R. A. 1981. Complementary rare earth element patterns in unique achondrites, such as ALH A77005 and shergottites, and in the earth. Proceedings, 12th Lunar and Planetary Science Conference. pp. 1349–1358.

Mason B. 1981. ALH A77005 petrographic description. *Antarctic Meteorite Newsletter* 4:12.

Mason B., MacPherson G. J., Score R., Martinez R., Satterwhite C., Schwarz C., and Gooding J. L. 1992. Descriptions of stony meteorites. In *Field and laboratory investigations of Antarctic meteorites collected by the United States expeditions 1985–1987,* edited by MacPherson M. and MacPherson G. J. Washington: Smithsonian Institution Press. 116 p.

McCoy T. J., Taylor G. J., and Keil K. 1992. Zagami: Product of a two-stage magmatic history. *Geochimica et Cosmochimica Acta* 56:3571–3582.

McSween H. Y., Jr. 1985. SNC meteorites: Clues to martian petrologic evolution. *Reviews of Geophysics* 23:391–416.

McSween H. Y., Jr. 2002. The rocks of Mars, from far and near. *Meteoritics & Planetary Science* 37:7–25.

McSween H. Y., Jr. and Keil K. 2000. Mixing relationships in the martian regolith and the composition of globally homogeneous dust. *Geochimica et Cosmochimica Acta* 64:2155–2166.

McSween H. Y., Jr., Taylor L. A., and Stolper E. M. 1979. Alan Hills 77055: A new meteorite type found in Antarctica. *Science* 204: 1201–1203.

Mellon M. T., Jakosky B. M., Kieffer H. H., and Christensen P. R. 2000. High resolution thermal inertia mapping from the Mars Global Surveyor thermal emission spectrometer. *Icarus* 148: 437–455.

Melosh H. J. 1985. Ejection of rock fragments from planetary bodies. *Geology* 13:144–148.

Mileikowsky C., Cucinotta F. A., Wilson J. W., Gladman B., Horneck G., Lindegren L., Melosh J., Rickman H., Valtonen M., and Zheng J. Q. 2000. Natural transfer of viable microbes in space. *Icarus* 145:391–427.

Mouginis-Mark P. J. 2002. Prodigious ash deposits near the summit of Arsia Mons volcano, Mars. *Geophysical Research Letters* 29: 15.

Mouginis-Mark P. J., McCoy T. J., Taylor G. J., and Keil K. 1992. Martian parent craters for the SNC meteorites. *Journal of Geophysical Research* 97:10213–10225.

Mustard J. F., Erard S., Bibring J. P., Head J. W., Hurtrez S., Langevin Y., Pieters C. M., and Sotin C. J. 1993. The surface of Syrtis Major: Composition of the volcanic substrate and mixing with altered dust and soil. *Journal of Geophysical Research* 98:3387–3400.

Mustard J. F., Murchie S. L., Erard S., and Sunshine J. M. 1997. In situ compositions of martian volcanics: Implications for the mantle. *Journal of Geophysical Research* 102:25605–25615.

Mustard J. F. and Sunshine J. M. 1995. Seeing through the dust: Martian crustal heterogeneity and links to the SNC meteorites. *Science* 267:1623–1626.

Nyquist L. E. 1983. Do oblique impacts produce martian meteorites? *Journal of Geophysical Research* 88:A785–A798.

Nyquist L. E. 1984. The oblique impact hypothesis and relative probabilities of lunar and martian meteorites. *Journal of Geophysical Research* 89:B631–B640.

Nyquist L. E., Bogard D. D., Shih C. Y., Greshake A., Stoffler D., and Eugster O. 2001. Ages and geologic histories of martian meteorites. *Chronology and Evolution of Mars* 96:105–164.

Nyquist L. E., Borg L. E., and Shih C. Y. 1998. The Shergottite age paradox and the relative probabilities for martian meteorites of differing ages. *Journal of Geophysical Research* 103:31445–31455.

O'Keefe J. D. and Ahrens T. J. 1986. Oblique impact: A process for obtaining meteorite samples from other planets. *Science* 234: 346–349.

Prinz M., Hlava P. H., and Keil K. 1974. The Chassigny meteorite: A relatively iron-rich cumulate dunite. *Meteoritics* 9:393–394.

Ramsey M. S. and Christensen P. R. 1998. Mineral abundance determination: Quantitative deconvolution of thermal emission spectra. *Journal of Geophysical Research* 103:577–596.

Rice J. W. Jr. 1997. Searching for the ALH 84001 "smoking gun" (parent crater) (abstract #1859). 28th Lunar and Planetary Science Conference. CD-ROM.

Rubin A. E., Warren P. H., Greenwood J. P., Verish R. S., Leshin L. A., Hervig R. L., Clayton R. N., and Mayeda T. K. 2000. Los Angeles: The most differentiated basaltic martian meteorite. *Geology* 28:1011–1014.

Ruff S. W. and Christensen P. R. 2002. Bright and dark regions on Mars: Particle size and mineralogical characteristics based on thermal emission spectrometer data. *Journal of Geophysical Research* 107:2-1.

Ruff S. W., Christensen P. R., Barbera P. W., and Anderson D. L. 1997. Quantitative thermal emission spectroscopy of minerals: A technique for measurement and calibration. *Journal of Geophysical Research* 102:14899–14913.

Ruff S. W. and Hamilton V. E. 2001. Mineralogical anomalies in Mars' Nili Patera caldera observed with thermal emission spectrometer data (abstract #2186). 32nd Lunar and Planetary Science Conference. CD-ROM.

Salisbury J. W., Walter L. S., Vergo N., and D'aria D. M. 1991. *Infrared (2.1–25 μm) spectra of minerals.* Baltimore: Johns Hopkins University Press. 267 p.

Schultz P. H. and Lutz-Garihan A. B. 1982. Grazing impacts on Mars: A record of lost satellites. *Journal of Geophysical Research* 87: A84–A96.

Singer R. B. 1980. The dark materials on Mars: I. New information from reflectance spectroscopy on the extent and mode of oxidation. 11th Lunar and Planetary Science Conference. pp. 1045–1047.

Singer R. B. and McSween H. Y., Jr. 1993. The igneous crust of Mars: Compositional evidence from remote sensing and the SNC meteorites. In *Resources of near-Earth space,* edited by Lewis J. S., Matthews M. S., and Guerrieri M. L. Tucson: University of Arizona Press. pp. 709–736.

Smith M. D., Bandfield J. L., and Christensen P. R. 2000. Separation of atmospheric and surface spectral features in Mars Global Surveyor thermal emission spectrometer (TES) spectra. *Journal of Geophysical Research* 105:9589–9607.

Stolper E. M. and McSween H. Y., Jr. 1979. Petrology and origin of the shergottite meteorites. *Geochimica et Cosmochimica Acta* 43: 1475–1498.

Thomson J. L. and Salisbury J. W. 1993. The mid-infrared reflectance of mineral mixtures (7–14 μm). *Remote Sensing of Environment* 45:1–13.

Treiman A. H. 1995. S≠NC: Multiple source areas for martian meteorites. *Journal of Geophysical Research* 100:5329–5340.

Treiman A. H., Gleason J. D., and Bogard D. D. 2000. The SNC meteorites are from Mars. *Planetary Space Science* 48:1213–1230.

Treiman A. H., McKay G. A., Bogard D. D., Wang M. S., Lipschutz M. E., Mittlefehldt D. W., Keller L., Lindstrom M. M., and Garrison D. 1994. Comparison of the LEW 88516 and

ALH A77005 martian meteorites: Similar but distinct. *Meteoritics* 29:581–592.

Vickery A. M. and Melosh H. J. 1987. The large crater origin of SNC meteorites. *Science* 237:738–743.

Vidal G. 1984. The oldest eukaryotic cells. *Scientific American* 250: 48–57.

Warren P. H. 1994. Lunar and martian meteorite delivery services. *Icarus* 111:338–363.

White B. 1979. Soil transport by winds on Mars. *Journal of Geophysical Research* 84:4643–4651.

Wood C. A. and Ashwal L. D. 1981. SNC meteorites: Igneous rocks from Mars? Proceedings, 12th Lunar and Planetary Science Conference. pp.1359–1375.

Wyatt M. B., Hamilton V. E., McSween H. Y., Jr., and Christensen P. R. 2001. Analysis of terrestrial and martian volcanic compositions using thermal emission spectroscopy: I. Determination of mineralogy, chemistry, and classification strategies. *Journal of Geophysical Research* 106:14711–14732.

Wyatt M. B. and McSween H. Y., Jr. 2002. Spectral evidence for weathered basalt as an alternative to andesite in the northern lowlands of Mars. *Nature* 417:263–266.

Zuber M. T., Solomon S. C., Phillips R. J., Smith D. E., Tyler G. L., Aharonson O., Balmino G., Banerdt W. B., Head J. W., Lemoine F. G., McGovern P. J., Neumann G. A., Rowlands D. D., and Zhong S. 2000. Internal structure and early thermal evolution of Mars from Mars Global Surveyor topography and gravity. *Science* 287:1788–1793.